

Communication

Exploring the Halogen-Bonded Cocrystallization Potential of a Metal–Organic Unit Derived from Copper(II) Chloride and 4-Aminoacetophenone

Vinko Nemec, Katarina Lisac, Marin Liović, Ivana Brekalo  and Dominik Cinčić * 

Department of Chemistry, Faculty of Science, University of Zagreb, Horvatovac 102a, HR-10000 Zagreb, Croatia; vnemec@chem.pmf.hr (V.N.); katarina.lisac@chem.pmf.hr (K.L.); marin.liovic1@gmail.com (M.L.); ivana.brekalo2@gmail.com (I.B.)

* Correspondence: dominik@chem.pmf.hr; Tel.: +385-1460-6362

Received: 22 April 2020; Accepted: 18 May 2020; Published: 22 May 2020



Abstract: In this work, we describe a novel halogen-bonded metal–organic cocrystal involving a square-planar Cu(II) complex and 1,4-diiodotetrafluorobenzene (**14tfib**) by utilizing an amine ligand whose pendant acetyl group enables halogen bonding. The cocrystal was prepared by both mechanochemical synthesis (liquid-assisted grinding) and the conventional solution-based method. Crystal structure determination by single crystal X-ray diffraction revealed that the dominant supramolecular interactions are the I...O halogen bond between **14tfib** and CuCl₂(**aap**)₂ building blocks, and the N–H...Cl hydrogen bonds between CuCl₂(**aap**)₂ molecules. The combination of halogen and hydrogen bonding leads to the formation of a 2D network. Overall, this work showcases an example of the possibility for extending the complexity of metal–organic crystal structures by using halogen bonding in a way that does not affect other hydrogen bonding synthons.

Keywords: halogen bonding; hydrogen bonding; cocrystals; liquid assisted grinding; coordination compounds

1. Introduction

In the past three decades, the halogen bond has increasingly proven itself as a supramolecular interaction that can be used alongside the well-researched hydrogen bond in crystal engineering [1–3]. Key points that allow this are: (a) the halogen bond is an attractive interaction between a positive area of electrostatic potential on covalently bound halogen atoms (Br, I) and Lewis bases (nucleophilic atoms such as O, N, S, Se, P, etc.) that ranges from weak to very strong (10–150 kJ mol^{−1}) [1,4,5], (b) it can be tuned by varying the donor atom used [6–9] or by changing its polarization [4,10] due to the fact that the halogen bond donor capacity results from the formation of a σ -hole, an electrophilic region, on the donor atom, (c) as a result, it is more directional than the hydrogen bond [1,4,6,11], and (d) it can form with acceptor atoms and species that are less receptive to hydrogen bonding [1,12,13]. These features of halogen bonding are especially interesting from the perspective of building larger acceptor molecules and more complex crystal structures, since they potentially provide a way to avoid synthon crossover that results from relying on only one interaction type [12,14].

While the majority of reports have focused on organic halogen-bonded crystals [1–3,10], the use of halogen bonding in the crystal engineering of metal–organic materials so far remains a challenge [15–19]. A number of reports and reviews have been published dealing with halogen bonding in single component metal–organic solids [15–17,20–23]. Most systematic studies of multicomponent metal–organic materials have focused on the utilization of halogen bonding with halide and pseudohalide (CN[−], SCN[−], OCN[−], and similar) ligands and ions, as they have shown to be reliable

in the synthesis of ionic metal–organic materials [24–33] and metal–organic cocrystals [15,34–36]. Several promising alternative approaches to obtaining neutral metal–organic materials have also recently been presented, generally focused on cocrystallizing neutral halogen bond donors with metal complex subunits that have either large chelating ligands (such as imines [37,38], acetylacetonates [39,40], or pyridine derivatives [41]) with pendant acceptor groups, or neutral monodentate ligands such as morpholine or thiomorpholine [42] coordinated to the metal complex. In all of the mentioned approaches an overwhelming majority of examples feature metal complex subunits that are chelated by bidentate (or tridentate) organic ligands. Searching the Cambridge Structural Database [43] for cocrystals of the selected iodoperfluorinated donors and metal–organic or organometallic species as halogen bond acceptors has resulted in a relatively small number of datasets (Table 1). The data obtained show that there are fewer cases where halogen bonds are formed with monodentate organic ligands than cases where they are formed with bidentate organic ligands, or directly bound halide or pseudohalide (CN^- , SCN^- , OCN^- , and similar) ligands. This is presumably because metal complexes that have monodentate ligands are less stable in solution in comparison to chelate metal complexes containing bidentate ligands [44], so the decomposition of the metal complex in solution significantly hinders the desired cocrystallization of the complex subunits with the halogen bond donor.

Table 1. The number of unique datasets in the Cambridge Structural Database (version 5.41, March 2020) corresponding to cocrystals of coordination compounds with the selected series of halogen bond donors [43].

Donor	Monodentate Ligand	Bidentate Ligand	Halide and Pseudohalide
1,4-diiidotetrafluorobenzene	8 hits	18 hits	20 hits
1,3-diiidotetrafluorobenzene	no hits	2 hits	2 hits
1,2-diiidotetrafluorobenzene	no hits	no hits	3 hits
1,3,5-triiidotrifluorobenzene	no hits	5 hits	2 hits

Our interest in the halogen bonding of coordination compounds is in the design and synthesis of extended structures, cocrystals, consisting of metal–organic complexes connected by halogen bonds. In our previous work, we have established that the peripherally located carbonyl functional group can function as a good halogen bond acceptor, allowing us to tune the properties of the material either via changing the metal center or the linking donor molecule [37,38]. Therein, we used a bidentate imine ligand in order to minimize or avoid the possibility of ligand detachment and separate cocrystallization with the donor molecules.

In this work, we were interested in testing the possibility of obtaining halogen-bonded cocrystals with coordination compounds featuring monodentate ligands. Additionally, we wanted to observe whether chloride ligands would hinder the formation of the desired halogen bond. To explore this, we have prepared a square-planar copper(II) complex that has both two chloride ligands and two 4-aminoacetophenone (**aap**) molecules as monodentate ligands, whose pendant acetyl group enables halogen bonding. For the cocrystal synthesis as halogen bond donors, we have selected a series of perhalogenated benzenes that differ in the number and positions of donor atoms: 1,4-diiidotetrafluorobenzene (**14tfib**), 1,3-diiidotetrafluorobenzene (**13tfib**), 1,2-diiidotetrafluorobenzene (**12tfib**), and 1,3,5-triiidotrifluorobenzene (**135tfib**) (Figure 1).

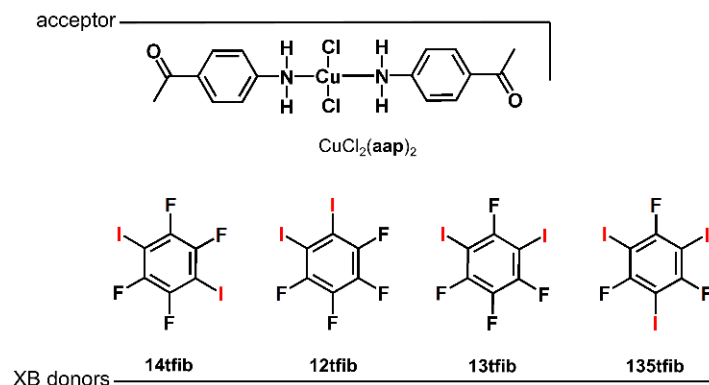


Figure 1. The halogen bond acceptor used in this study, a coordination compound derived from copper(II) chloride and 4-aminoacetophenone, and halogen bond donors, perhalogenated benzenes.

2. Materials and Methods

2.1. Synthesis of $\text{CuCl}_2(\text{aap})_2$

Copper(II) chloride dihydrate (1.00 g, 5.88 mmol) and **aap** (1.58 g, 11.8 mmol) were mixed with 30.0 mL of methanol in a round-bottom flask and stirred while heating under reflux for 1.0 h. The obtained crystals were filtered and washed with acetone.

2.2. Mechanochemical Experiments

In order to explore the cocrystallization of $\text{CuCl}_2(\text{aap})_2$ with selected halogen bond donors, we performed mechanochemical experiments by liquid-assisted grinding (LAG) [45,46] of the reactants in a 1:1 donor : complex stoichiometric ratio, and in the presence of a small amount of acetonitrile (see ESI, Table S1). Milling was conducted under normal laboratory conditions (temperature ca. 25 °C, 40–60% relative humidity) for 30 min in a Retsch MM200 Shaker Mill (Retsch GmbH, Haan, Germany) operating at 25 Hz frequency, using a 10 mL plexiglass jar and two stainless steel balls 7 mm in diameter. All reactants and products were characterized by powder X-ray diffraction (PXRD).

The $[\text{CuCl}_2(\text{aap})_2](\mathbf{14tfib})$ cocrystal was prepared by milling a mixture of 99.6 mg (0.246 mmol) $\text{CuCl}_2(\text{aap})_2$ and 100.0 mg (0.248 mmol) **14tfib** for 30 min along with 20.0 μL of ethanol.

2.3. Crystallization Experiments

A $\text{CuCl}_2(\text{aap})_2$ single crystal was obtained by slow evaporation at room temperature of the solution obtained by reflux synthesis. The $[\text{CuCl}_2(\text{aap})_2](\mathbf{14tfib})$ single crystal was obtained after dissolving a mixture of $\text{CuCl}_2(\text{aap})_2$ (50.0 mg, 0.123 mmol) and **14tfib** (50.0 mg, 0.124 mmol) in 5.0 mL of a hot mixture of tetrahydrofuran and ethanol (volume ratio 1:2) and the subsequent cooling and solvent evaporation at room temperature for two days.

2.4. Thermal Analysis

Thermal measurements were performed on a Mettler–Toledo TGA/DSC 3+ module (Mettler-Toledo, Greifensee, Switzerland). Samples were placed in open 70 μL alumina pans and heated from 25 to 600 °C at a rate of 10 °C min^{-1} under an oxygen flow of 50 mL min^{-1} . The data collection and analysis were performed using the program package STARe Software v15.00 (Mettler-Toledo GmbH, Giessen, Germany) [47].

2.5. Single-Crystal X-ray Diffraction Experiments

The crystal and molecular structures of the prepared samples were determined by single crystal X-ray diffraction. The details of the data collection and crystal structure refinement are listed in Table S2. The diffraction data for $\text{CuCl}_2(\text{aap})_2$ and $[\text{CuCl}_2(\text{aap})_2](\mathbf{14tfib})$ were collected at

295 K. Diffraction measurements were made on an Oxford Diffraction Xcalibur Kappa CCD X-ray diffractometer with graphite-monochromated MoK α ($\lambda = 0.71073 \text{ \AA}$) radiation. The datasets were collected using the ω scan mode over the 2θ range up to 54° . The programs CrysAlis CCD and CrysAlis RED (Oxford Diffraction Ltd., Abingdon, UK) were employed for data collection, cell refinement, and data reduction [48,49]. The structures were solved by direct methods and refined using the SHELXS, SHELXT, and SHELXL programs, respectively [50,51]. Structural refinement was performed on F² using all data. Hydrogen atoms not involved in hydrogen bonding were placed in calculated positions and treated as riding on their parent atoms [$d(\text{C-H}) = 0.93 \text{ \AA}$ and $U_{\text{iso}}(\text{H}) = 1.2 U_{\text{eq}}(\text{C})$], while the others were located from the electron difference map. Parameters of the supramolecular interactions that are present in the prepared compounds are listed in Table S3. All calculations were performed using the WinGX crystallographic suite of programs [52]. The images of the molecular structures of compounds and their molecular packing projections were prepared by Mercury [53].

2.6. Powder X-ray Diffraction Experiments

PXRD experiments on the samples were performed on a PHILIPS PW 1840 X-ray diffractometer (Philips Analytical, Almelo, The Netherlands) with CuK α 1 (1.54056 \AA) radiation at 40 mA and 40 kV. The scattered intensities were measured with a scintillation counter. The angular range was from 3 to 40° (2θ) with steps of $0.02\text{--}0.03^\circ$, and the measuring time was 0.2–0.5 s per step. Data collection and analysis was performed using the program package Philips X'Pert (Philips Analytical, Almelo, The Netherlands) [54–56].

3. Results and Discussion

The CuCl₂(**aap**)₂ complex was synthesized by reacting copper(II) chloride dihydrate and the **aap** ligand. The structure was confirmed by X-ray diffraction on crystals grown from the solution obtained by reflux synthesis (see ESI, Figure S5). Our screening for cocrystal formation of the obtained complex was based on mechanochemical liquid-assisted grinding followed by PXRD analysis. Only one out of a total of four reactant combinations resulted in the formation of new crystalline products, as evidenced by the appearance of new Bragg reflections in the PXRD patterns upon milling (see ESI, Figure S1). A new product is formed by milling CuCl₂(**aap**)₂ with **14tfib** in the presence of a small amount (40.0 μL) of acetonitrile (Figure 2). In the other cases (see ESI, Figures S2–S4), the PXRD pattern obtained shows either a reactant mixture (milling with **135tfib**), a reactant mixture that includes the appearance of several new Bragg peaks (milling with **12tfib** in both stoichiometric ratios), or peaks of CuCl₂(**aap**)₂ (milling with **13tfib**). The LAG experiment with CuCl₂(**aap**)₂ and **14tfib** was accompanied by crystallization from an ethanolic solution of the reagents which resulted in single crystals suitable for X-ray diffraction. Given our previous experiences in cocrystallization from solutions of metal complexes that have monodentate ligands, it was quite astonishing that we were able to obtain crystals of the desired product, the [CuCl₂(**aap**)₂](**14tfib**) cocrystal. For example, our previous attempt to cocrystallize **14tfib** with a similar Cu(II) complex derived from copper(II) chloride and 4-nitroaniline resulted in the crystallization of a cocrystal of free 4-nitroaniline and **14tfib** [57]. The measured PXRD pattern of the new mechanochemical product was found to be in good agreement with the patterns calculated from the single crystal X-ray diffraction of [CuCl₂(**aap**)₂](**14tfib**) (Figure 2), showing that the mechanochemically prepared cocrystal was obtained as a pure single phase. Similar experiments for the potential cocrystallization of CuCl₂(**aap**)₂ and **12tfib** from the reagent solution yielded only separate reactant phases.

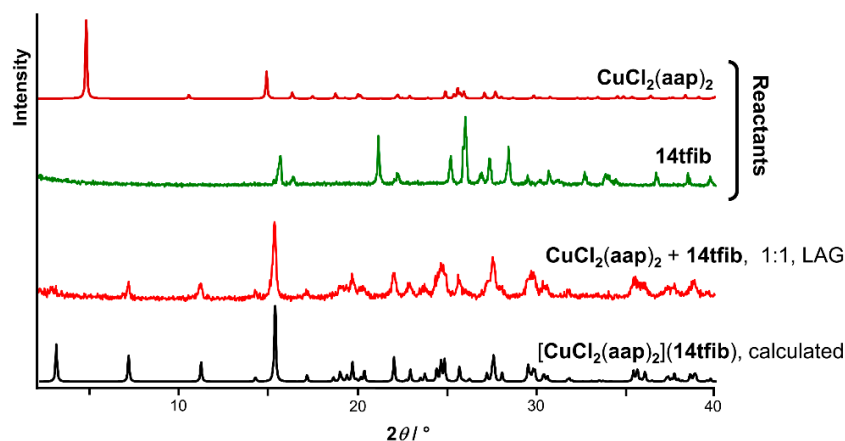


Figure 2. A comparison of the powder X-ray diffraction patterns of the reactants, the LAG product, and the pattern calculated from the $[\text{CuCl}_2(\text{aap})_2](14\text{tfib})$ single crystal X-ray diffraction data.

The molecular and crystal structure determination revealed that the asymmetric unit of $[\text{CuCl}_2(\text{aap})_2](14\text{tfib})$ contains one half of a $\text{CuCl}_2(\text{aap})_2$ molecule and one half of a 14tfib molecule (Figure 3). The molecular structure of the $\text{CuCl}_2(\text{aap})_2$ unit is in good agreement with that in the parent complex, with a root mean square deviation value of 0.1418 (see ESI, Figure S6). The central Cu(II) atom has a square planar coordination geometry and is coordinated by two N atoms from two aap molecules and two Cl atoms, forming a structure with a square planar geometry ($d(\text{Cu1-N1}) = 2.021 \text{ \AA}$, $d(\text{Cu1-Cl1}) = 2.251 \text{ \AA}$, $\angle(\text{N1-Cu1-Cl1}) = 88.8^\circ$ and 91.2° , $\tau_4 = \tau_4' = 0$) [58,59].

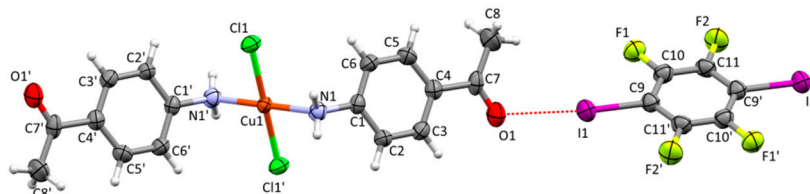


Figure 3. Molecular structure of $[\text{CuCl}_2(\text{aap})_2](14\text{tfib})$ showing the atom-labelling scheme. Displacement ellipsoids are drawn at a 50% probability level, and H atoms are shown as small spheres of arbitrary radius (See ESI, Table S4, for the symmetry codes of symmetry equivalent atoms marked with an ' symbol).

In the crystal structure, each $\text{CuCl}_2(\text{aap})_2$ unit is associated with two 14tfib molecules via almost linear $\text{I}\cdots\text{O}$ halogen bonds ($d(\text{I1}\cdots\text{O1}) = 2.988 \text{ \AA}$, $\angle(\text{C1-I9}\cdots\text{O1}) = 173^\circ$), forming halogen-bonded chains (Figure 4a). This halogen bond can be considered relatively strong, as evidenced not only by its linearity, but also by the relatively large value of the donor \cdots acceptor distance shortening, 14.6%, with respect to the sum of the corresponding van der Waals radii of atoms [60]. Each coordinated Cl atom is only involved as an acceptor in $\text{N-H}\cdots\text{Cl}$ hydrogen bonding ($d(\text{N1}\cdots\text{Cl1}) = 3.466 \text{ \AA}$, $\angle(\text{N1-H1A}\cdots\text{Cl1}) = 165^\circ$) with the amino group of an adjacent molecule, similar to the $\text{CuCl}_2(\text{aap})_2$ parent complex (Figure 4b). We therefore conclude that there appears to be no competition between the chloride ligand and the carbonyl functional group for halogen bonding with 14tfib . The combination of halogen and hydrogen bonding leads to the formation of layers (Figure 4a). The overall structure results from the stacking of such layers along the $[3\ 0\ 13]$ crystallographic direction (Figure 4c).

Importantly, the $\text{CuCl}_2(\text{aap})_2$ parent complex also forms supramolecular chains, where the $\text{CuCl}_2(\text{aap})_2$ units—instead of being bridged by halogen bonding with 14tfib molecules—are directly bound into a chain through pairs of $\text{C-H}\cdots\text{O}$ hydrogen bonds forming $R_2^2(8)$ motifs ($d(\text{C8}\cdots\text{O1}) = 3.61 \text{ \AA}$, $\angle(\text{C8-H8C}\cdots\text{O1}) = 168.0^\circ$) (Figure 4b). These supramolecular chains are again connected into a layer by a combination of $\text{N-H}\cdots\text{Cl}$ hydrogen bonds ($d(\text{N1}\cdots\text{Cl1}) = 3.474 \text{ \AA}$, $\angle(\text{N1-H2N}\cdots\text{Cl1}) = 171^\circ$). The final crystal structure is built by further stacking of the layers along the $[5\ 0\ 14]$ crystallographic direction

(Figure 4d). We hypothesize that this similarity between the crystal structures of the parent complex and the halogen-bonded cocrystal is the reason why **14tfib** easily forms a cocrystal with $\text{CuCl}_2(\text{aap})_2$ in solution and mechanochemically, while other halogen bond donors of similar size and donor strength do not.

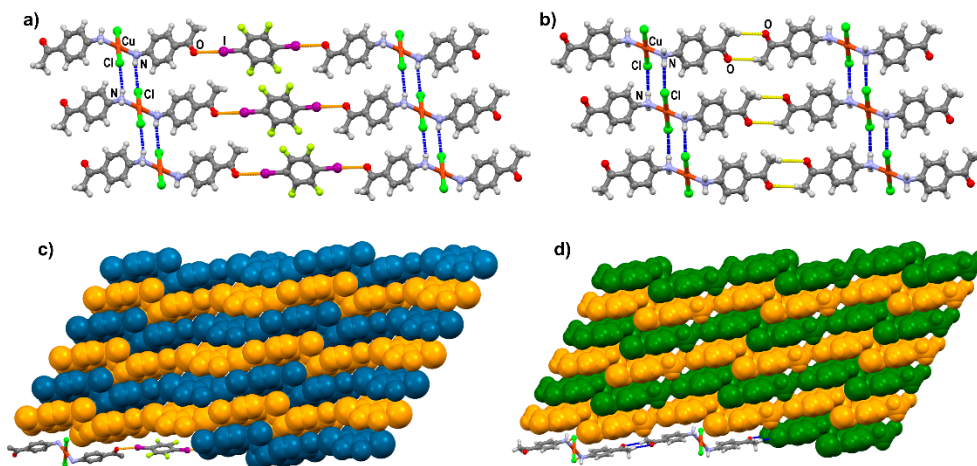


Figure 4. Parts of the crystal structure of (a) $[\text{CuCl}_2(\text{aap})_2](\mathbf{14tfib})$ showcasing the 2D network formed by a combination of halogen (colored orange) and hydrogen bonds (colored blue), (b) $\text{CuCl}_2(\text{aap})_2$ with the 2D network resulting from a combination of $\text{N-H}\cdots\text{Cl}$ and $\text{C-H}\cdots\text{O}$ hydrogen bonds (colored blue and yellow, respectively). Layer stacking in (c) $[\text{CuCl}_2(\text{aap})_2](\mathbf{14tfib})$ and (d) $\text{CuCl}_2(\text{aap})_2$. For clarity, adjacent layers are color-coded orange and blue/green.

The thermal analysis by TGA reveals that the parent coordination compound and its halogen-bonded cocrystal decompose upon heating in two steps. Evaluating the inflection point temperature for the first step of thermal degradation (see ESI, Figures S7 and S8) reveals that both compounds have similar thermal stabilities, 137 °C for $\text{CuCl}_2(\text{aap})_2$ and 145 °C for $[\text{CuCl}_2(\text{aap})_2](\mathbf{14tfib})$. The similarity in thermal degradation temperature is interesting, considering their different compositions and supramolecular architectures, as well as the fact that the pure halogen bond donor, **14tfib**, has a melting point of ~108 °C.

4. Conclusions

To conclude, we have successfully obtained a cocrystal with a one-dimensional halogen-bonded metal–organic architecture, using a copper(II) coordination compound that has a monodentate ligand with peripherally located carbonyl oxygen atoms. As in our previous work, the carbonyl oxygen of the acetyl group has proven its potential as a good halogen bond acceptor, although the present study indicates that its potential can be severely limited by other effects. In the case of the $\text{CuCl}_2(\text{aap})_2$ complex, a molecule with a linear distribution of donor atoms (such as **14tfib**) can replace the $\text{C-H}\cdots\text{O}$ hydrogen bonding motif of the parent complex by insertion. Other molecules of similar size and donor strength, but with donor atoms at an angle, like **12tfib**, **13tfib**, and **135tfib**, cannot because their incorporation would require a significant alteration of the overall crystal structure and connectivity. Disrupting the strong $\text{N-H}\cdots\text{Cl}$ hydrogen bond motif connecting the supramolecular chains would be especially difficult and severely limits the number of acceptable donor molecules. Furthermore, the strong $\text{N-H}\cdots\text{Cl}$ hydrogen bond motif effectively ‘masks’ the chloride ligand, preventing it from competing with the acetyl group for halogen bond formation. To overcome these limitations and further explore the competitiveness of halides with peripherally located ligands for halogen bonding, our future research will focus on systems with hydrogen bond-donating functional groups that are weaker than the amino group.

Supplementary Materials: The following are available online at <http://www.mdpi.com/1996-1944/13/10/2385/s1>, Figure S1: PXRD patterns of (a) $\text{CuCl}_2(\text{aap})_2$, (b) **14tfib**, (c) product obtained by grinding $\text{CuCl}_2(\text{aap})_2$ and **14tfib** in a 1:1 stoichiometric ratio, (d) calculated pattern from $[\text{CuCl}_2(\text{aap})_2](\text{14tfib})$ single crystal data, Figure S2: PXRD patterns of (a) $\text{CuCl}_2(\text{aap})_2$, (b) **12tfib**, (c) product obtained by grinding $\text{CuCl}_2(\text{aap})_2$ and **12tfib** in a 1:2 stoichiometric ratio, (d) product obtained by grinding $\text{CuCl}_2(\text{aap})_2$ and **12tfib** in a 1:1 stoichiometric ratio. Stars denote small peaks not belonging to either reactant, Figure S3: PXRD patterns of (a) $\text{CuCl}_2(\text{aap})_2$, (b) product obtained by grinding $\text{CuCl}_2(\text{aap})_2$ and **13tfib** in a 1:1 stoichiometric ratio, Figure S4: PXRD patterns of (a) **135tfib**, (b) $\text{CuCl}_2(\text{aap})_2$, (c) product obtained by grinding $\text{CuCl}_2(\text{aap})_2$ and **135tfib** in a 1:1 stoichiometric ratio, Figure S5: Molecular structure of $\text{CuCl}_2(\text{aap})_2$ showing the atom-labelling scheme. Displacement ellipsoids are drawn at the 50% probability level, and H atoms are shown as small spheres of arbitrary radius. Symmetry codes of symmetry equivalent atoms marked with an ' symbol are listed in Table S4, Figure S6: Molecular overlay of the metal complex molecule obtained from $\text{CuCl}_2(\text{aap})_2$ data (colored red) with the metal complex molecule obtained from $[\text{CuCl}_2(\text{aap})_2](\text{14tfib})$ data (colored blue). The metal complex structures are in good agreement with a root mean square deviation (RMSD) value of 0.1418 and a maximum distance of 0.2619, Figure S7: TG and DSC curves of $\text{CuCl}_2(\text{aap})_2$, Figure S8: TG and DSC curves of $[\text{CuCl}_2(\text{aap})_2](\text{14tfib})$, Table S1: Mechanochemical synthesis parameters, Table S2: Crystal data and refinement details for the prepared compounds, Table S3: Parameters of the supramolecular interactions and corresponding symmetry operators present in the prepared compounds, Table S4: Atom list and symmetry codes of symmetry equivalent atoms (marked with an ' symbol) in the prepared compounds. CCDC 1997629 and 1997630 contain crystallographic data for this paper. These data can be obtained free of charge from the Director, CCDC, 12 Union Road, Cambridge, CBZ 1EZ, UK (Fax: +44-1223-336033; email: deposit@ccdc.cam.ac.uk or <http://www.ccdc.cam.ac.uk>).

Author Contributions: Synthesis of the parent Cu(II) complex, I.B.; Cocrystal synthesis, D.C. and V.N.; Mechanochemical experiments, K.L. and M.L.; Characterization and single-crystal X-ray diffraction analysis, K.L. and V.N.; Writing—original draft preparation, D.C. and V.N. All authors have read and agreed to the published version of the manuscript.

Funding: This research was supported by the Croatian Science Foundation under projects HRZZ-IP-2014-09-7367 and HRZZ-IP-2019-04-1868.

Conflicts of Interest: There are no conflict to declare.

References

1. Cavallo, G.; Metrangolo, P.; Milani, R.; Pilati, T.; Priimagi, A.; Resnati, G.; Terraneo, G. The Halogen Bond. *Chem. Rev.* **2016**, *116*, 2478–2601. [[CrossRef](#)]
2. Fourmigué, M. Halogen bonding: Recent advances. *Curr. Opin. Solid State Mater. Sci.* **2009**, *13*, 36–45. [[CrossRef](#)]
3. Priimagi, A.; Cavallo, G.; Metrangolo, P.; Resnati, G. The Halogen Bond in the Design of Functional Supramolecular Materials: Recent Advances. *Acc. Chem. Res.* **2013**, *46*, 2686–2695. [[CrossRef](#)] [[PubMed](#)]
4. Politzer, P.; Murray, J.S.; Clark, T. Halogen bonding: An electrostatically-driven highly directional noncovalent interaction. *Phys. Chem. Chem. Phys.* **2010**, *12*, 7748–7757. [[CrossRef](#)] [[PubMed](#)]
5. Lisac, K.; Topić, F.; Arhangeliskis, M.; Cepić, S.; Julien, P.A.; Nickels, C.W.; Morris, A.J.; Friščić, F.; Cinčić, D. Halogen-bonded cocrystallization with phosphorus, arsenic and antimony acceptors. *Nat. Commun.* **2019**, *10*, 61. [[CrossRef](#)]
6. Legon, A.C. The halogen bond: An interim perspective. *Phys. Chem. Chem. Phys.* **2010**, *12*, 7736–7747. [[CrossRef](#)]
7. Messina, M.T.; Metrangolo, P.; Panzeri, W.; Ragg, E.; Resnati, G. Perfluorocarbon-hydrocarbon self-assembly. Part 3. Liquid phase interactions between perfluoroalkylhalides and heteroatom containing hydrocarbons. *Tetrahedron Lett.* **1998**, *39*, 9069–9072. [[CrossRef](#)]
8. Cinčić, D.; Friščić, T.; Jones, W. Isostructural materials achieved by using structurally equivalent donors and acceptors in halogen-bonded cocrystals. *Chem. Eur. J.* **2008**, *14*, 747–753. [[CrossRef](#)]
9. Stilinović, V.; Horvat, G.; Hrenar, T.; Nemeč, V.; Cinčić, D. Halogen and hydrogen bonding between (N-halogeno) succinimides and pyridine derivatives in solution, the solid state and in silico. *Chem. Eur. J.* **2017**, *23*, 5244–5257. [[CrossRef](#)]
10. Troff, R.W.; Mäkelä, T.; Topić, F.; Valkonen, A.; Raatikainen, K.; Rissanen, K. Alternative motifs for halogen bonding. *Eur. J. Org. Chem.* **2013**, *9*, 1617–1637. [[CrossRef](#)]
11. Eraković, M.; Cinčić, D.; Molčanov, K.; Stilinović, V. Crystallographic Charge Density Study of the Partial Covalent Nature of Strong N...Br Halogen Bonds. *Angew. Chem. Int. Ed.* **2019**, *58*, 15702–15706. [[CrossRef](#)] [[PubMed](#)]

12. Aakeröy, C.B.; Schultheiss, N.C.; Rajbanshi, A.; Desper, J.; Moore, C. Supramolecular synthesis based on a combination of hydrogen and halogen bonds. *Cryst. Growth Des.* **2009**, *9*, 432–441. [[CrossRef](#)] [[PubMed](#)]
13. Aakeröy, C.B.; Wijethunga, T.K.; Haj, M.A.; Desper, J.; Moore, C. The structural landscape of heteroaryl-2-imidazoles: Competing halogen- and hydrogen-bond interactions. *CrystEngComm* **2014**, *16*, 7218–7225. [[CrossRef](#)]
14. Aakeröy, C.B.; Chopade, P.D.; Desper, J. Avoiding “synthon crossover” in crystal engineering with halogen bonds and hydrogen bonds. *Cryst. Growth Des.* **2011**, *11*, 5333–5336. [[CrossRef](#)]
15. Bertani, R.; Sgarbossa, P.; Venzo, A.; Lelj, F.; Amati, M.; Resnati, G.; Pilati, T.; Metrangolo, P.; Terraneo, G. Halogen bonding in metal–organic–supramolecular networks. *Coord. Chem. Rev.* **2010**, *254*, 677–695. [[CrossRef](#)]
16. Mahmudov, K.T.; Kopylovich, M.N.; Guedes da Silva, M.F.C.; Pompeiro, A.J.L. Non-covalent interactions in the synthesis of coordination compounds: Recent advances. *Coord. Chem. Rev.* **2017**, *345*, 54–72. [[CrossRef](#)]
17. Li, B.; Zhang, S.-Q.; Wang, L.-Y.; Mak, T.C.W. Halogen bonding: A powerful, emerging tool for constructing high-dimensional metal-containing supramolecular networks. *Coord. Chem. Rev.* **2016**, *308*, 1–21. [[CrossRef](#)]
18. Gamekkanda, J.C.; Sinha, A.S.; Desper, J.; Đaković, M.; Aakeröy, C.B. The Role of Halogen Bonding in Controlling Assembly and Organization of Cu (II)-Acac Based Coordination Complexes. *Crystals* **2017**, *7*, 226. [[CrossRef](#)]
19. Aakeröy, C.B.; Schultheiss, N.; Desper, J.; Moore, C. Attempted assembly of discrete coordination complexes into 1-D chains using halogen bonding or halogen···halogen interactions. *CrystEngComm* **2007**, *9*, 421–426. [[CrossRef](#)]
20. Zordan, F.; Brammer, L.; Sherwood, P. Supramolecular Chemistry of Halogens: Complementary features of inorganic (M–X) and organic (C–X′) halogens applied to M–X···X′–C halogen bond formation. *J. Am. Chem. Soc.* **2005**, *127*, 5979–5989. [[CrossRef](#)]
21. Brammer, L.; Espallargas, G.M.; Libri, S. Combining metals with halogen bonds. *CrystEngComm* **2008**, *10*, 1712–1727. [[CrossRef](#)]
22. Nandi, G.; Titi, H.M.; Goldberg, I. Exploring supramolecular self-assembly of metalloporphyrin tectons by halogen bonding. 2. *Cryst. Growth Des.* **2014**, *14*, 3557–3566. [[CrossRef](#)]
23. Fernandez-Palacio, F.; Saccone, M.; Priimagi, A.; Terraneo, G.; Pilati, T.; Metrangolo, P.; Resnati, G. Coordination networks incorporating halogen-bond donor sites and azobenzene groups. *CrystEngComm* **2016**, *18*, 2251–2257. [[CrossRef](#)]
24. Espallargas, G.M.; Brammer, L.; Sherwood, P. Designing intermolecular interactions between halogenated peripheries of inorganic and organic molecules: Electrostatically directed M–X···X′–C halogen bonds. *Angew. Chem. Int. Ed.* **2006**, *45*, 435–440. [[CrossRef](#)]
25. Awwadi, F.F.; Willett, R.D.; Twamley, B. The aryl chlorine-halide ion synthon and its role in the control of the crystal structures of tetrahalocuprate(II) ions. *Cryst. Growth Des.* **2007**, *7*, 624–632. [[CrossRef](#)]
26. Derossi, S.; Brammer, L.; Hunter, C.A.; Ward, M.D. Halogen bonded supramolecular assemblies of [Ru(bipy)(CN)₄]²⁻ anions and *N*-methyl-halopyridinium cations in the solid state and in solution. *Inorg. Chem.* **2009**, *48*, 1666–1677. [[CrossRef](#)]
27. Valle, G.; Ettore, R. Bis(4-bromoimidazolium) tetrachloropalladate(II). *Acta Cryst. C* **1994**, *50*, 1221–1222. [[CrossRef](#)]
28. Imakubo, T.; Sawa, H.; Kato, R. Novel molecular conductors, (DIETS)₄M(CN)₄ (M = Ni, Pd, Pt): Highly reticulated donor···anion contacts by –I···NC– interaction. *J. Chem. Soc. Chem. Commun.* **1995**, *16*, 1667–1668. [[CrossRef](#)]
29. Yamashita, Y.; Tomura, M.; Badruz-Zaman, M. Synthesis and properties of novel tetrathiafulvalene vinylogues. *Chem. Commun.* **1998**, *16*, 1657–1658. [[CrossRef](#)]
30. Kosaka, Y.; Yamamoto, H.M.; Tajima, A.; Nakao, A.; Cui, H.; Kato, R. Supramolecular Ni(dmit)₂ salts with halopyridinium cations -development of multifunctional molecular conductors with the use of competing supramolecular interactions. *CrystEngComm* **2013**, *15*, 3200–3211. [[CrossRef](#)]
31. Imakubo, T.; Kobayashi, M. Effects of solvent additives on the crystal architecture of supramolecular conductors based on diiodo(ethylenedithio)tetraselenafulvalene and indium tetrahalide anions. *Eur. J. Inorg. Chem.* **2014**, *24*, 3973–3981. [[CrossRef](#)]

32. Pfrunder, M.C.; Micallef, A.S.; Rintoul, L.; Arnold, D.P.; McMurtrie, J. Interplay between the supramolecular motifs of polypyridyl metal complexes and halogen bond networks in cocrystals. *Cryst. Growth Des.* **2016**, *16*, 681–695. [[CrossRef](#)]
33. Jeon, I.-R.; Mathonière, C.; Clérac, R.; Rouzières, M.; Jeannin, O.; Trzop, E.; Collet, E.; Fourmigué, M. Photoinduced reversible spin-state switching of an Fe^{III} complex assisted by a halogen-bonded supramolecular network. *Chem. Commun.* **2017**, *53*, 10283–10286. [[CrossRef](#)] [[PubMed](#)]
34. Ding, X.; Tuikka, M.J.; Hirva, P.; Kukushkin, V.Y.; Novikov, A.S.; Haukka, M. Fine-tuning halogen bonding properties of diiodine through halogen-halogen charge transfer- extended [Ru(2,2'-bipyridine)(CO)₂X₂]-I₂ systems (X = Cl, Br, I). *CrystEngComm* **2016**, *18*, 1987–1995. [[CrossRef](#)]
35. Ivanov, D.M.; Novikov, A.S.; Ananyev, I.V.; Kirina, Y.V.; Kukushkin, V.Y. Halogen bonding between metal centers and halocarbons. *Chem. Commun* **2016**, *52*, 5565–5568. [[CrossRef](#)] [[PubMed](#)]
36. Lisac, K.; Cinčić, D. Simple design for metal-based halogen-bonded cocrystals utilizing the M–Cl⋯I motif. *CrystEngComm* **2018**, *20*, 5955–5963. [[CrossRef](#)]
37. Cinčić, D.; Friščić, T. Synthesis of an extended halogen-bonded metal–organic structure in a one-pot mechanochemical reaction that combines covalent bonding, coordination chemistry and supramolecular synthesis. *CrystEngComm* **2014**, *16*, 10169–10172. [[CrossRef](#)]
38. Nemeč, V.; Fotović, L.; Friščić, T.; Cinčić, D. A large family of halogen-bonded cocrystals involving metal-organic building blocks with open coordination sites. *Cryst. Growth Des.* **2017**, *17*, 6169–6173. [[CrossRef](#)]
39. Merkens, C.; Pan, F.; Englert, U. 3-(4-pyridyl)-2,4-pentanedione - a bridge between coordinative, halogen, and hydrogen bonds. *CrystEngComm* **2013**, *15*, 8153–8158. [[CrossRef](#)]
40. Pfrunder, M.C.; Brock, A.J.; Brown, J.J.; Grosjean, A.; Ward, J.; McMurtrie, J.C.; Clegg, J.K. A three-dimensional cubic halogen-bonded network. *Chem. Commun.* **2018**, *54*, 3974–3976. [[CrossRef](#)]
41. Ghosh, B.N.; Lahtinen, M.; Kalenius, E.; Mal, P.; Rissanen, K. 2,2':6',2''-terpyridine trimethylplatinum(IV) iodide complexes as bifunctional halogen bond acceptors. *Cryst. Growth Des.* **2016**, *16*, 2527–2534. [[CrossRef](#)]
42. Lapadula, G.; Judaš, N.; Friščić, T.; Jones, W. A three-component modular strategy to extend and link coordination complexes by using halogen bonds to O, S and π acceptors. *Chem. Eur. J.* **2010**, *16*, 7400–7403. [[CrossRef](#)] [[PubMed](#)]
43. Groom, C.R.; Bruno, I.J.; Lightfoot, M.P.; Ward, S.C. The Cambridge Structural Database. *Acta Cryst. B* **2016**, *72*, 171–179. [[CrossRef](#)] [[PubMed](#)]
44. Kettle, S.F.A. Stability of coordination compounds. In *Physical Inorganic Chemistry*; Springer: Berlin/Heidelberg, Germany, 1996; pp. 73–94.
45. James, S.L.; Adams, C.J.; Bolm, C.; Braga, D.; Collier, P.; Friščić, T.; Grepioni, F.; Harris, K.D.M.; Hyett, G.; Jones, W.; et al. Mechanochemistry: Opportunities for new and cleaner synthesis. *Chem. Soc. Rev.* **2012**, *41*, 413–447. [[CrossRef](#)] [[PubMed](#)]
46. Friščić, T.; Jones, W. Recent advances in understanding the mechanism of cocrystal formation via grinding. *Cryst. Growth Des.* **2009**, *9*, 1621–1637. [[CrossRef](#)]
47. *STARe Evaluation Software Version 15.00 (Build 8668)*, Mettler-Toledo GmbH: Giessen, Germany, 2016.
48. *CrysAlis CCD V171.34*, Oxford Diffraction, Oxford Diffraction Ltd.: Abingdon, Oxfordshire, UK, 2003.
49. *CrysAlis RED V171.34*, Oxford Diffraction, Oxford Diffraction Ltd.: Abingdon, Oxfordshire, UK, 2003.
50. Sheldrick, G.M. A short history of SHELX. *Acta Cryst. A* **2008**, *64*, 112–122. [[CrossRef](#)]
51. Sheldrick, G.M. SHELXT- Integrated space-group and crystal-structure determination. *Acta Cryst. A* **2015**, *71*, 3–8. [[CrossRef](#)]
52. Farrugia, L.J. WinGX suite for small-molecule single-crystal crystallography. *J. Appl. Cryst.* **1999**, *32*, 837–838. [[CrossRef](#)]
53. Macrae, C.F.; Bruno, I.J.; Chisholm, J.A.; Edgington, P.R.; McCabe, P.; Pidcock, E.; Rodriguez-Monge, L.; Taylor, R.; van de Streek, J.; Wood, P.A. *Mercury CSD 2.0*- new features for the visualization and investigation of crystal structures. *J. Appl. Cryst.* **2008**, *41*, 466–470. [[CrossRef](#)]
54. *Philips X'Pert Data Collector 1.3e*, Philips Analytical, B.V.: Almelo, The Netherlands, 2001.
55. *Philips X'Pert Graphics & Identify 1.3e*, Philips Analytical, B.V.: Almelo, The Netherlands, 2001.
56. *Philips X'Pert Plus 1.0*, Philips Analytical, B.V.: Almelo, The Netherlands, 1999.

57. Nemeč, V.; Cinčić, D. Uncommon halogen bond motifs in cocrystals of aromatic amines and 1,4-diodotetrafluorobenzene. *CrystEngComm* **2016**, *18*, 7425–7429. [[CrossRef](#)]
58. Yang, L.; Powell, D.R.; Houser, R.P. Structural variation in copper(I) complexes with pyridylmethanamide ligands: Structural analysis with a new four-coordinate geometry index, τ_4 . *Dalton Trans.* **2007**, 955–964. [[CrossRef](#)] [[PubMed](#)]
59. Okuniewski, A.; Rosiak, D.; Chojnacki, J.; Becker, B. Coordination polymers and molecular structures among complexes of mercury(II) halides with selected 1-benzoylthioureas. *Polyhedron* **2015**, *90*, 47–57. [[CrossRef](#)]
60. Bondi, A.J. van der Waals volumes and radii. *Phys. Chem.* **1964**, *68*, 441–451. [[CrossRef](#)]



© 2020 by the authors. Licensee MDPI, Basel, Switzerland. This article is an open access article distributed under the terms and conditions of the Creative Commons Attribution (CC BY) license (<http://creativecommons.org/licenses/by/4.0/>).